

Electromagnetic dissociation of ^{238}U at 120 MeV/nucleon

M. L. Justice, Y. Blumenfeld,* N. Colonna,[†] D. N. Delis, G. Guarino,
K. Hanold, J. C. Meng,[‡] G. F. Peaslee,[§] G. J. Wozniak, and L. G. Moretto

Lawrence Berkeley Laboratory, Berkeley, California 94720

(Received 19 November 1992; revised manuscript received 2 June 1993)

Electromagnetic fission cross sections of a 120 MeV/nucleon ^{238}U beam incident on five targets, ^9Be , ^{27}Al , $^{\text{nat}}\text{Cu}$, $^{\text{nat}}\text{Ag}$, and $^{\text{nat}}\text{U}$, have been extracted from measurements of projectile velocity fission fragments. The nuclear interaction contributions to the experimentally observed cross sections were determined by extrapolation from the Be target data using a geometrical scaling model and by an empirical decomposition of the fission charge distributions. The results are compared to model calculations in which electric quadrupole excitations have been included.

PACS number(s): 25.70.Jj

Electromagnetic dissociation (EMD) is a process that occurs when a nucleus is excited above its particle emission threshold by the electromagnetic field induced by another nucleus as it passes by outside the range of the strong nuclear force. Experimentally, electromagnetic dissociation has been observed with relativistic heavy ions [1–17]. Aside from the emulsion work of Ref. [6], however, these experiments have been restricted to either few nucleon removal from heavy nuclei or several nucleon removal from light nuclei. Here we present the results of the first electronic counter experiment designed to measure electromagnetic fission cross sections of a heavy nucleus. In addition, this was the first measurement of EMD cross sections at a beam energy where there is predicted to be a significant contribution from electric quadrupole excitations.

Fission cross sections of a 120 MeV/nucleon ^{238}U beam incident on five targets (^9Be , ^{27}Al , $^{\text{nat}}\text{Cu}$, $^{\text{nat}}\text{Ag}$, and $^{\text{nat}}\text{U}$) were measured at the Lawrence Berkeley Laboratory's BEVALAC. The projectile velocity fission fragments were detected in coincidence by 16 position sensitive ΔE - E telescopes [18]. Each telescope was composed of a 300 μm diffused junction Si ΔE detector followed by a 5 mm Si(Li) E detector. The telescopes were placed concentrically about the beam in two rings of eight telescopes each. The upstream ring intersected the beam axis 37.0 cm downstream of the target and covered the angular region $4.5^\circ \lesssim \theta \lesssim 13.5^\circ$, while the downstream ring intersected the beam axis 103.2 cm downstream of the target and covered $1.5^\circ \lesssim \theta \lesssim 4.5^\circ$. One surface of each silicon detector was divided into fifteen 2.42 mm wide, high conductivity strips separated by 0.607 mm wide, high resistivity gaps to give position information through the technique of resistive charge division. The strips of the E detectors were rotated 90° with respect

to the ΔE strips to give full two-dimensional position information with an overall resolution of ~ 1.5 mm in the x and y directions. The absolute beam flux was measured with a 1/4 in. thick plastic scintillator paddle located approximately 150 cm downstream of the target. A complete description of the experimental setup along with the details of the procedure used to calibrate the silicon detectors can be found in Ref. [19].

Pulse height information from the E and ΔE detectors was combined, using a range algorithm [20], to determine the charges of the fragments. The charge resolution obtained varied from approximately $\pm 0.25 Z$ units for the lightest fission fragments to approximately $\pm 0.5 Z$ units for the heaviest fragments. The position information from the Si detectors was used, along with the total energy deposited, to determine the velocity vectors of the fragments.

Raw $Z_1 + Z_2$ distributions for the five targets are shown in Fig. 1. The range of excitation energies associated with virtual photon absorption is modest (< 20 MeV) at the beam energy of this experiment. Therefore, electromagnetic fission practically always leads to a true charge sum of 92. Of course, the data also contain a large background from nuclear interaction processes in which there can be much larger energy transfers and/or transfer of charge. The ratio of electromagnetic to nuclear fragmentation is expected to increase with the charge of the target nucleus, however, as can be seen in the increasing sharpness of the peak at $Z_1 + Z_2 = 92$ as Z_{target} increases in Fig. 1.

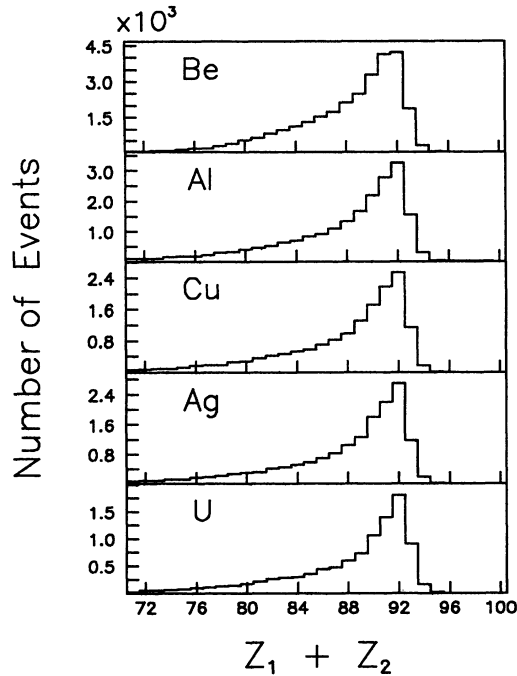
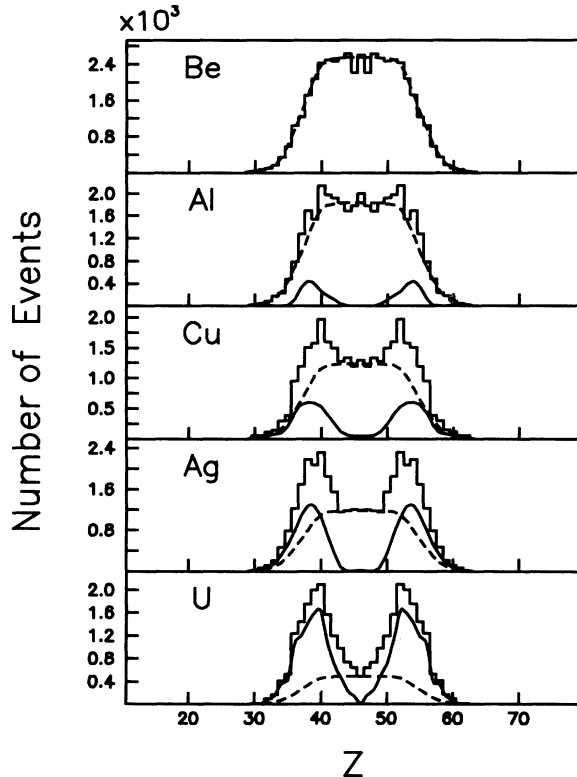
Acceptance corrected Z distributions for $Z_1 + Z_2 = 92$ events are shown in Fig. 2. A smooth transition from primarily symmetric fission for the Be target data to primarily asymmetric fission for the U target data is seen. As is well known from studies of light-particle induced fission, the magnitude of the asymmetric component in fragment yields is a sensitive function of the amount of excitation energy imparted to the fissioning system [21]. Higher excitation energies lead to increased yields of the symmetric component in ^{238}U fission. Quantitative estimates of the energy transfers from the data of Fig. 2 are complicated by fragment charge misidentification, but loose limits can be derived. From a comparison of the Z distributions of Fig. 2 with experimental data on ^{238}U fission fragment

*Present address: Institute de Physique Nucleaire, Orsay, France.

[†]Present address: INFN, Bari, Italy.

[‡]On leave from the Institute of Atomic Energy, Beijing, China.

[§]Present address: NSCL, MSU, East Lansing, MI 48844.


 FIG. 1. Raw $Z_1 + Z_2$ distributions.

 FIG. 2. Acceptance corrected Z distributions for $Z_1 + Z_2 = 92$ events. The dashed and solid curves represent the nuclear and EMD contributions to the yield. See discussion in text.

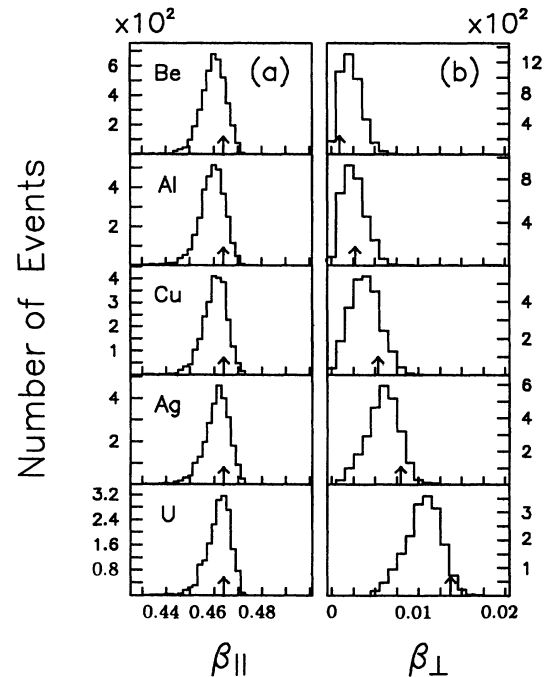
yields vs excitation energy [22], the conclusion is that $\langle E_{\text{exc}} \rangle \geq 50$ MeV for the Be data and $\langle E_{\text{exc}} \rangle \leq 36$ MeV for the U data.

For the most peripheral events ($Z_1 + Z_2 = 91, 92, 93$), a velocity for the fissioning source was calculated assuming two body decay:

$$\vec{\beta}_s = \frac{\vec{P}_s}{[P_s^2 + M_s^2]^{1/2}}, \quad (1)$$

where $\vec{P}_s \equiv \vec{p}_1 + \vec{p}_2$ and $M_s \equiv M_1 + M_2$. Plots of the parallel and transverse components of $\vec{\beta}_s$ for $Z_1 + Z_2 = 92$ events are shown in Fig. 3. Although the β_{\parallel} distributions for the five targets look very similar, the β_{\perp} distributions shift to larger values as the target atomic number increases. This behavior can be explained as being due to the increasing Coulomb kick the projectile receives from the target by the Rutherford scattering term in the potential. For reference, the arrows in Fig. 3(b) indicate the transverse velocities one would expect from classical Rutherford trajectories at grazing impact parameters, b_{graze} , calculated from Eq. (7) below. For the heaviest targets, and especially for U, most events fall inside the classical grazing angle. The cross section for electromagnetic fission should be peaked at b_{graze} with a tail extending toward larger impact parameters. However, since the fissioning source cannot be expected to follow an exact Coulomb trajectory at this beam energy, the precise relationship between b and β_{\perp} is unknown.

The geometrical acceptances of the detector system for coincidence events leading to charge sums of 91, 92, and 93 were calculated with a Monte Carlo program. The


 FIG. 3. (a) Parallel source velocities for $Z_1 + Z_2 = 92$ events. The arrows mark the beam velocity. (b) Transverse source velocities for $Z_1 + Z_2 = 92$ events. The arrows mark the calculated transverse velocities assuming classical Rutherford trajectories at $b = b_{\text{min}}$.

fragments were assumed to be emitted isotropically in the projectile rest frame with kinetic energies taken from measurements on proton-induced ^{238}U fission [23]. A grid of 20×20 points covering the measured range of β_{\perp} vs β_{\parallel} was set up and 100 000 events for each $Z_1 - Z_2$ split were generated at each point. Coincidence efficiencies at other values of $\vec{\beta}_s$ were determined by interpolation. Total fission cross sections for $Z_1 + Z_2 = 92$ events in mb were then calculated from the relation

$$\sigma_{92}^f = \sum_{i,j=92-i} \frac{n_{ij}A}{\epsilon_{ij}F\Delta xN_A} \times 10^{30}, \quad (2)$$

where n_{ij} and ϵ_{ij} are the number of detected events and coincidence efficiency for $Z_1 = i$, $Z_2 = j$ as a function of $\vec{\beta}_s$, A is the atomic weight of the target, F is the integrated beam flux, Δx is the thickness of the target in mg/cm^2 , and N_A is Avogadro's number. Total fission cross sections for $Z_1 + Z_2 = 91$ and $Z_1 + Z_2 = 93$ events were calculated from similar expressions.

Due to the imperfect charge resolution of our detectors, we cannot give reliable values for the cross sections into individual fragmentation channels. Detailed Monte Carlo studies of the effects of charge misidentification were made, however, and it was found that the sum cross sections

$$\sigma_{\Sigma}^f = \sigma_{91}^f + \sigma_{92}^f + \sigma_{93}^f \quad (3)$$

were relatively insensitive ($< 6\%$) to fragment Z misidentification [19]. Moreover, it was determined that $< 5\%$ of the true $Z_1 + Z_2 = 92$ events were misidentified by more than one charge sum unit, indicating that nearly all of the electromagnetic fission events are included in σ_{Σ}^f .

The sum cross sections include a nuclear interaction component as well as the EMD component:

$$\sigma_{\Sigma}^f = \sigma_{\text{EMD}}^f + \sigma_{\text{nuc}}^f. \quad (4)$$

Under the conditions of this experiment, the cross section for the Be target data is expected to be almost entirely due to nuclear interaction. The nuclear cross sections for the other four targets were determined from the Be data using a simple geometrical scaling model:

$$\sigma_{\text{nuc}}^{\text{geom}} = 2\pi \left(b_{\text{min}} - a - \frac{\Delta b}{2} \right) \Delta b, \quad (5)$$

where

$$a = \frac{Z_p Z_t e^2}{\mu \beta^2 \gamma} \quad (6)$$

corrects for the Rutherford bending of the trajectory [19]. Using the parametrization [24]

$$b_{\text{min}} = 1.34 \left[A_p^{1/3} + A_t^{1/3} - 0.75 \left(A_p^{-1/3} + A_t^{-1/3} \right) \right], \quad (7)$$

and the measured cross section of 494 ± 11 mb for the Be data, Δb was determined to be $\Delta b = 0.80 \pm 0.04$ fm.

The EMD fission cross sections obtained by subtracting off the extrapolated nuclear cross sections are listed in Table I under $\sigma_{\text{exp}}^{\text{I}}$ and plotted as circles in Fig. 4. The error bars for the Al, Cu, and Ag target cross sec-

TABLE I. Experimental and calculated EMD fission cross sections (mb).

Target	$\sigma_{\text{exp}}^{\text{I}}$	$\sigma_{\text{exp}}^{\text{II}}$	σ_{WW}	σ_{E1+E2}
Al	78 ± 30	43	27	33
Cu	246 ± 37	190	99	120
Ag	393 ± 42	361	204	248
U	568 ± 127	811	504	613

tions were calculated from the statistical uncertainties plus the best estimate of the uncertainties introduced by fragment charge misidentification. The large error on the U target point includes an additional uncertainty introduced by problems with the beam flux counter during this run. All errors are 1σ . The overall normalization uncertainty of Fig. 4 is estimated to be $\pm 20\%$. Errors due to uncertainties in the extrapolation of the nuclear fragmentation cross sections are difficult to estimate and are not included. The method used here to extrapolate σ_{nuc} is essentially the same as has been used previously in other EMD experiments, however.

We have also attempted to extract the EMD cross sections through a graphical decomposition of the Z distributions of Fig. 2. The dashed curves represent the approximate nuclear contributions if one assumes that the shape of the nuclear component for all targets is the same as the Be distribution. The approximate EMD components were obtained by subtracting the dashed curves from the histograms. The solid curves of Fig. 2 show the smoothed results. For the particular decomposition shown in the figure, the fraction of $Z_1 + Z_2 = 92$ events attributable to electromagnetic dissociation ranges from less than 10% for Al to $\sim 70\%$ for U.

In order to derive cross sections from the decompositions of Fig. 2 the $Z_1 + Z_2 = 92$ events that were misidentified as having a charge sum of 91 or 93 must be accounted for. Assuming that the true 92 charge sum events were equally likely to be misidentified as 91's or

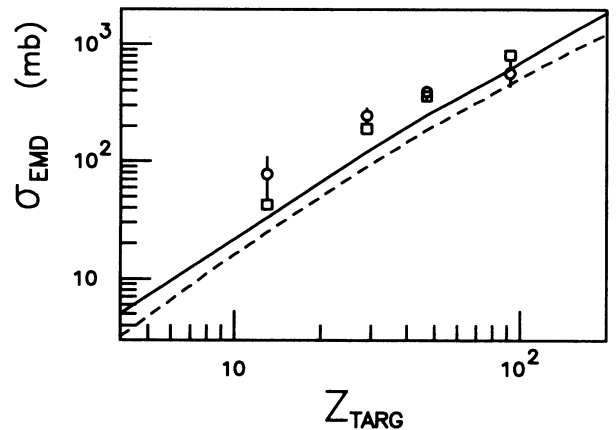


FIG. 4. Experimental EMD cross sections extracted from σ_{Σ}^f (circles) and from the graphical decomposition of Fig. 2 (squares). The dashed curve is the WW prediction. The solid curve was obtained by summing over $E1$ and $E2$ multipoles. The log-log plot emphasizes the approximate Z_{TARG} dependence contained in Eqs. (9) and (11).

93's and that the true cross section for $Z_1 + Z_2 = 93$ is negligible, one has

$$\sigma_{92}^{\text{true}} \approx \sigma_{92}^{\text{obs}} + 2 \times \sigma_{93}^{\text{obs}} .$$

The EMD cross sections arrived at by this alternative method are listed in Table I under $\sigma_{\text{exp}}^{\text{II}}$ and plotted as squares in Fig. 4. Because of the very rough and qualitative nature of the graphical decomposition no attempt has been made to assign errors to the $\sigma_{\text{exp}}^{\text{II}}$ values. The $\sigma_{\text{exp}}^{\text{II}}$ values are all within 2σ of the $\sigma_{\text{exp}}^{\text{I}}$ values, however.

A framework for calculating EMD cross sections is given by the equivalent photon approximation [25]:

$$\sigma_{\text{EMD}} = \int d\omega \sigma_{\gamma}(\omega) N(\omega) , \quad (8)$$

where $\sigma_{\gamma}(\omega)$ is the appropriate photodissociation cross section for the fragmenting nucleus and $N(\omega)$ is the virtual photon spectrum generated by the other nucleus.

The simplest form of the virtual photon spectrum is given by the Weizsäcker-Williams (WW) approximation [26]. In the WW approach the classical electromagnetic fields are approximated as two pulses of plane waves. The resulting number spectrum of virtual photons per unit photon energy interval, integrated over impact parameters, is given by

$$N^{\text{WW}}(\omega) = \frac{2Z^2\alpha}{\pi\omega\beta^2} \left[\xi K_0(\xi) K_1(\xi) - \frac{\beta^2\xi^2}{2} [K_1^2(\xi) - K_0^2(\xi)] \right] , \quad (9)$$

where ω is the virtual photon energy, Z is the charge of the nucleus emitting the virtual photon, β is the relative velocity of the two nuclei, K_0 (K_1) is the modified Bessel function of order zero (one), $\xi = \omega b_{\text{min}}/\beta\gamma$, and b_{min} is the cutoff impact parameter, below which nuclear fragmentation processes take over and electromagnetic dissociation ceases to be important.

An approach that goes beyond the WW approximation has been given by Alder and Winther [27], and later put into the context of the virtual photon language by Bertulani and Baur [28]. In this approach, a proper multipole expansion of the electromagnetic field is made and an analytical expression for the equivalent photon numbers of all multipoles is obtained. Equation (8) is then modified to read

$$\sigma_{\text{EMD}} = \sum_{\pi l} \int d\omega \sigma_{\gamma}^{\pi l}(\omega) N^{\pi l}(\omega) , \quad (10)$$

where $\sigma_{\gamma}^{\pi l}(\omega)$ is the photodissociation cross section for real photons of multipolarity πl . The expression for $N^{E1}(\omega)$ in this multipole expansion method is identical to $N^{\text{WW}}(\omega)$, while the $E2$ spectrum is given by [28]

$$N^{E2}(\omega) = \frac{2Z^2\alpha}{\pi\omega\beta^4} \left[2(1-\beta^2) K_1^2 + (2-\beta^2)^2 \xi K_0 K_1 - \frac{\xi^2\beta^4}{2} (K_1^2 - K_0^2) \right] , \quad (11)$$

where all K 's are functions of ξ as in Eq. (9). In the high energy limit, as $\beta \rightarrow 1$, Eq. (11) becomes equivalent to Eq. (9). In fact, this is true in general; as the velocity of the projectile approaches the speed of light, the virtual

photon spectra for all multipoles become equivalent to the $E1$ spectrum. At lower relative velocities, however, $N^{E2}(\omega)$ can be significantly enhanced in comparison to $N^{\text{WW}}(\omega)$.

The curves in Fig. 4 are the results of two model calculations. The lower, dashed curve is the prediction of the WW approximation with the parametrization of Eq. (7) for b_{min} . The total photofission cross section was taken from Ref. [29]. The upper, solid curve was calculated by summing over $E1$ and $E2$ multipoles using Eq. (10). The $E2$ photoabsorption cross section was assumed to be of the form [30]

$$\sigma_{\gamma}^{E2}(\omega) = \frac{8\pi^3\alpha}{150(\hbar c)^2} \omega^3 \frac{dB^{E2}}{d\omega} , \quad (12)$$

with the following form for the strength function, $dB^{E2}/d\omega$,

$$\frac{dB^{E2}}{d\omega} = \frac{K}{\omega} \frac{\Gamma^2}{(\omega^2 - \omega_0^2)^2 + \omega^2\Gamma^2} . \quad (13)$$

The value of K was determined by assuming that the $E2$ cross section exhausts 100% of the energy-weighted sum rule [30]:

$$\int d\omega \omega \frac{dB^{E2}}{d\omega} = \frac{25\hbar^2 Z^2}{4\pi AM} \langle R^2 \rangle , \quad (14)$$

where M is the nucleon mass, Z and A are the charge and mass number of ^{238}U , and $\langle R^2 \rangle$ is its mean square radius. The numerical value of the right-hand side of this equation was taken to be $1.00 \times 10^5 \text{ MeV fm}^4$ [31]; ω_0 and Γ were taken to be 10 MeV and 3.5 MeV, respectively [32].

The $E2$ photofission cross section is related to the total $E2$ photoabsorption cross section by

$$\sigma_{\gamma,f}^{E2}(\omega) = P_f^{E2}(\omega) \sigma_{\gamma}^{E2}(\omega) , \quad (15)$$

where $P_f^{E2}(\omega)$ is the $E2$ fission probability as a function of photon energy. The parametrization

$$P_f^{E2}(\omega) = a - \frac{b}{1 + e^{(\omega-c)/d}} , \quad (16)$$

with $a = 0.4$, $b = 0.18$, $c = 13.4 \text{ MeV}$, and $d = 0.59 \text{ MeV}$ was used for $P_f^{E2}(\omega)$. This parametrization reproduces the total fission probability as measured in photonuclear experiments [33]. The recoil correction to the equivalent photon numbers [27]

$$b_{\text{min}} \longrightarrow b_{\text{min}} + \frac{\pi}{2} a , \quad (17)$$

where a is given by Eq. (6), was included in both of the calculations of Fig. 4.

A potentially important deficiency of the models is their neglect of nuclear deformation effects. For a ^{238}U projectile incident on a spherical target, the effect would enter through a dependence of b_{min} on the particular orientation of the projectile. In the case where the target is also deformed there could be an additional effect on the multipole structure of the fields generated by the target.

A proper treatment of these two effects would involve a complicated averaging over the various possible orientations of the projectile and target and has not been attempted. Qualitatively, however, it is clear that the first effect would serve to increase the theoretical predictions, since allowing b_{\min} to depend on orientation increases the number of events at smaller impact parameters. As for the second effect, it is not obvious in which direction or by how much the various equivalent photon numbers would be shifted but if, for example, $N^{E1}(\omega)$ is decreased at the expense of higher multipoles then the cross section for a deformed target would go down.

While the experimental cross sections extracted by method I are seen to increase with Z_{targ} in Fig. 4, the quantitative agreement with the model calculations is only fair. The Al, Cu, and Ag data points have approximately the correct Z_{targ} dependence but lie well above the theoretical predictions, while the U point is clearly too low in relation to the other points. A 2σ shift upward of the U point gives the data approximately the same shape as the solid curve, only too high by $\sim 50\%$ — well above the estimated normalization uncertainty.

Both the overall normalization and the Z_{targ} dependence of the cross sections extracted by method II agree more closely with the model predictions.

In summary, we have demonstrated a new technique for studying the electromagnetic dissociation process. The trend in fragment mass asymmetries of Fig. 2 provides conclusive evidence of an electromagnetic component to the total fission cross sections of ^{238}U at 120 MeV/nucleon. The extracted electromagnetic fission cross sections are not inconsistent with calculations which include electric quadrupole excitations. However, the sensitivity of this experiment to the quadrupole component is limited by the uncertainty in the evaluation of the nuclear contributions. More data on ^{238}U fission at other beam energies are needed in order to reduce this uncertainty.

This work was supported by the Director, Office of Energy Research, Division of Nuclear Physics of the Office of High Energy and Nuclear Physics of the U.S. Department of Energy under Contract DE-AC03-76SF00098.

-
- [1] H.H. Heckman and P.J. Lindstrom, *Phys. Rev. Lett.* **37**, 56 (1976).
 - [2] G.D. Westfall *et al.*, *Phys. Rev. C* **19**, 1309 (1979).
 - [3] D.L. Olson *et al.*, *Phys. Rev. C* **24**, 1529 (1981).
 - [4] M.T. Mercier *et al.*, *Phys. Rev. Lett.* **52**, 898 (1984).
 - [5] M.T. Mercier *et al.*, *Phys. Rev. C* **33**, 1655 (1986).
 - [6] L.F. Canto *et al.*, *Phys. Rev. C* **35**, 2175 (1987).
 - [7] J.C. Hill *et al.*, *Phys. Rev. Lett.* **60**, 999 (1988).
 - [8] J.C. Hill *et al.*, *Phys. Rev. C* **38**, 1722 (1988).
 - [9] P.B. Price *et al.*, *Phys. Rev. Lett.* **61**, 2193 (1988).
 - [10] C. Brechtmann and W. Heinrich, *Z. Phys. A* **330**, 407 (1988).
 - [11] C. Brechtmann and W. Heinrich, *Z. Phys. A* **331**, 463 (1988).
 - [12] J.C. Hill *et al.*, *Phys. Rev. C* **39**, 524 (1989).
 - [13] C. Brechtmann *et al.*, *Phys. Rev. C* **39**, 2222 (1989).
 - [14] G. Baroni *et al.*, *Nucl. Phys.* **A516**, 673 (1990).
 - [15] D.L. Olson *et al.*, *Phys. Rev. C* **44**, 1862 (1991).
 - [16] J.C. Hill *et al.*, *Phys. Lett. B* **273**, 371 (1991).
 - [17] R. Schmidt *et al.*, *Phys. Rev. Lett.* **70**, 1767 (1993).
 - [18] W.L. Kehoe *et al.*, *Nucl. Instrum. Methods* **A311**, 258 (1992).
 - [19] M.L. Justice, Ph.D. thesis, University of California, Berkeley, 1991; Lawrence Berkeley Laboratory Report LBL-31704.
 - [20] F.S. Goulding and B.G. Harvey, *Annu. Rev. Nucl. Sci.* **25**, 167 (1975).
 - [21] R. Vandenbosch and J.R. Huizenga, *Nuclear Fission* (Academic Press, New York, 1973).
 - [22] R. Vandenbosch *et al.*, *Phys. Rev. Lett.* **52**, 1964 (1984).
 - [23] R.L. Ferguson *et al.*, *Phys. Rev. C* **7**, 2510 (1973).
 - [24] C.J. Benesh *et al.*, *Phys. Rev. C* **40**, 1198 (1989).
 - [25] C.A. Bertulani and G. Baur, *Phys. Rep.* **163**, 299 (1988).
 - [26] C.F. Weizsäcker, *Z. Phys.* **88**, 612 (1934); E.J. Williams, *Phys. Rev.* **45**, 729 (1934).
 - [27] A. Winther and K. Alder, *Nucl. Phys.* **A319**, 518 (1977).
 - [28] C.A. Bertulani and G. Baur, *Nucl. Phys.* **A442**, 739 (1985).
 - [29] J.T. Caldwell *et al.*, *Phys. Rev. C* **21**, 1215 (1980).
 - [30] J.S. O'Connell, in *Proceedings of the International Conference on Photoneuclear Reactions and Applications*, edited by B.L. Berman (Lawrence Livermore Laboratory, Livermore, CA, 1973), p. 71.
 - [31] Th. Weber *et al.*, *Phys. Rev. Lett.* **59**, 2028 (1987).
 - [32] J.D.T. Arruda-Neto and B.L. Berman, *Phys. Scr.* **40**, 735 (1989).
 - [33] A. Veyssièrè *et al.*, *Nucl. Phys.* **A199**, 45 (1973).